Out-of-plane behavior of reinforced masonry walls: Experimental and numerical study

Natalino Gattesco, Ingrid Boem*

University of Trieste, Department of Engineering and Architecture, Italy

ARTICLE INFO

Accepted 1 July 2017

Keywords:
Masonry structures
Seismic retrofitting
Structural rehabilitation
Composite materials
Glass-fibers
Out-of-plane behavior
Finite element analysis

ABSTRACT

In the paper, the results of an experimental and numerical study on the out-of-plane bending effectiveness of a modern strengthening technique applied to existing masonry walls are presented. The technique consists in the application, on both wall faces, of a mortar coating reinforced with glass fiber-reinforced polymer (GFRP) meshes. Four point bending tests of full scale masonry samples (1000 width, 3000 mm height) were carried out considering three types of masonry (solid brick, 250 mm thick, rubble stone and cobblestones, 400 mm thick). The performances of plain and reinforced specimens were analysed and compared. It emerged that strengthened specimens are able to resist out-of-plane bending moments almost 4–5 times greater than those of plain specimens; moreover they can overcome deflections more than 25 times higher, due to the presence of the GFRP mesh, which contrasts the opening of cracks. The cracking and the ultimate bending moments of reinforced samples can be analytically predicted using relationships quite close to those used in the design of reinforced concrete beams subjected to combined axial and bending actions. The results of nonlinear static analyses performed on a 2D numerical model were also presented, so to comprehend the mechanical behaviour of reinforced masonry walls. Their agreement with the experimental results proved the reliability of the simulations; moreover, the extension of the 2D model to a 3D one, necessary to analyze the behavior of perforated walls, was also made.

1. Introduction

The aim to preserve ancient masonry buildings, due to their cultural and historical relevance, is often accompanied by the necessity to improve the structural safety of this architectural heritage. In particular, an important topic is to overcome to structural deficiencies related to earthquakes, as, in general, seismic provisions were not considered in the construction of these buildings. The past seismic events evidenced the poor performances of these structures (composed mainly of unreinforced masonry walls made of brick or stone units, jointed together through weak lime mortars, and wooden floors) which led to partial or global collapse due to the out-of-plane (in bending) or in-plane failure (in shear or bending) of the walls. The main critical aspects are related, on one side, to the material characteristics, such as the masonry high mass (high inertia forces) and the low masonry tensile strength and, on the other end, to structural deficiencies, such as the lack of effective connections among the resisting elements, the presence of horizontal thrust transmitted by arches, vaults and roofs, the inappropriate distribution of the walls in the two main direction and the in-plane deformability of timber horizontal diaphragms (repartition of the seismic forces proportional to the masses).

In most cases, the out-of-plane failure may be inhibited providing an adequate in-plane stiffness to the floors (e.g. by means of nailed steel plates, glued fiber reinforced polymer (FRP) strips or reinforced concrete subfloor anchored to the timber joists [1]) and an effective connection among perpendicular walls and between the walls and the horizontal diaphragms (e.g. through reinforced concrete tie beams, steel tie rods or angles [2]). Once these structural deficiencies have been amended, attaining, thus, to the so called “box behavior”, the distribution of the seismic action among the vertical resisting elements depends on their stiffness and the building failure is generally due to the in-plane collapse of the masonry walls. However, in masonry structures with high interstorey distance (4–5 m), the out-of-plane bending actions may be relevant, constituting a great problem especially in upper storeys of tall buildings, where the out-of-plane forces are higher, the axial

* Corresponding author.
E-mail addresses: gattesco@units.it (N. Gattesco), boem@dicar.units.it (I. Boem).

load is reduced and, frequently, walls are thinner than those at lower levels.

Several techniques have been extensively applied in the past for the enhancement of both the in-plane and out of-plane performances of masonry walls, most concerning in the application of concrete coatings with steel meshes embedded (such as ferrocement [3,4], reinforced cement-based plasters [5,6] and shotcrete overlays [7,8]) or in the insertion of steel ties or strips in the mortar joints or in cuts created near the masonry surface, before repointing [9]. These reinforcements were proved as able to provide to the masonry both high strength and a properly ductile behaviour. In particular, the presence of the steel reinforcement permits the improvement of the wall deformation capacity. However, the contribution of the reinforcement can be vanished by the premature detachment of the reinforcement from the masonry [10,11], as the distribution of the seismic actions depends on the stiffness ratio between the two materials. It is thus of fundamental relevance to provide a good bond of the coating or repointing (e.g. cleaning, saturation, mechanical or chemical treatment of the masonry surface) and, if necessary, an adequate dimensioning of connectors. Moreover, severe steel corrosion problems emerged in several cases, over the time. For this reason, traditional retrofitting techniques were gradually replaced, in the last twenty years, by different reinforcement solutions based on no-corrosive materials such as FRP, based mostly on carbon, glass or aramid fibers [12,13], PBO (polybenzoxazole) [14], PP (polypropylene) [15] or stainless steel [16,17]. The fundamental benefits of the reinforcement with a composite material are strictly related to its great performances when subjected in tension.

The first application experiences in the use of FRP for the strengthening of existing masonry concerned mostly in the external bonding of thin fabrics, strips or laminates of FRP to the wall surface by impregnation with epoxy resin matrix [18–21]. Several experimental campaigns were aimed to assess the effectiveness of this technique against out-of-plane actions and to evaluate the influence on its effectiveness of different parameters as the fiber type and amount, the type of resin, the reinforcement arrangement and the boundary conditions (e.g. Refs. [22–25]). Externally bonded (EB) FRP results an effective technique and has the advantage to not increase the building mass. Typically, the benefits of the EB FRP reinforcement are related to the ability of the composite material in contrasting the opening of masonry cracks, due to the high tensile strength. However, some drawbacks have to be considered: some tests evidenced that FRP is not totally compatible with the masonry, due to the differences between stiffness, strengths and thermal coefficients. In fact, in the application on masonry surfaces, the technique frequently evidenced a poor bond to the substrate (due to the higher surface roughness and irregularity, in respect to concrete) which may induce the reinforcement delamination, reducing the effectiveness of the intervention [26–29]. In addition the epoxy resins, besides being high-costs and requiring special handling equipment and skilled installation staff, have very scarce resistance to high-temperatures and fire and are affected by ultraviolet (UV), water and alkaline degradation, needing therefore adequate protection systems [30–32]. Moreover, their application on wet surfaces or at low temperatures is not possible. Furthermore, the difficulty in removal the intervention (irreversibility of the retrofitting) lead heritage conservation authorities to avoid its application on listed historical buildings.

Thus, alternative effective rehabilitation strategies, based on the use of FRP bars or strips, mounted near the wall surface (NSM – near surface mounted) in epoxy-filled grooves created in the masonry, were developed [33–37]. In these cases, the composite is less exposed to the environment condition and fire and the visual impact of the intervention upon the structure is minimal; the premature failure of the reinforcement by pull-out may however occur [38].

Other valid reinforcement methods, able to overcome most of the limits of FRP, concern fiber-reinforced cementitious matrix (FRCM) and fiber-reinforced mortars (FRM – known also as FRG - fiber reinforced grouts - or TRM - textile reinforced mortars), where the FRP elements are embedded in an inorganic matrix [39–42]. The various proposed systems differ in the type and thickness of the matrix (ranging from high strength cement-based mixtures to natural lime mortars, from a 10 mm thin layer of scratch coat to a 30–40 mm thick layer) and in the characteristics of the FRP reinforcement (mostly textile or meshes). The installation approach is quite simple, as requires the same skills and instruments of a traditional reinforced coating intervention, such as ferrocement or steel-reinforced plasters. These strengthening systems generally exhibit a more effective bond with the substrate in respect to the epoxy glued fibers techniques and also better performances at elevated temperatures [43–45]. Inorganic matrices have a higher compatibility with historic masonry and, especially when lime-based mortars are employed, do not prejudice its water and vapour permeability (avoiding, thus, dangerous moisture accumulation at the interface) and the reversibility of the intervention.

Some experimental investigations on masonry walls strengthened through the application of a mortar coating reinforced with textiles or preformed composite meshes evidenced the capacity of these reinforcement systems to increase the out-of-plane resistance of masonry [46–49], also raising significantly the plastic deformation capacity. However, the masonry-matrix bonding performances still remain a key topic for an effective design of the material [55]. Shear bond tests [50,51] permit to evaluate the interaction between the composite material and the masonry substrate and are typically based on small masonry samples (single brick, stone units or masonry wallets) to which the reinforcement is applied on one or both sides, for a determined area. Variations in the nature and roughness of the masonry surface, in the bond area and in the characteristics of the composite material, influence the resistance and the type of collapse [52–54]. To avoid the detachment of wall coatings and to improve the reinforcement effectiveness, transversal mechanical connectors were also introduced in some applications.

The experimental investigations available in the literature on the out-of-plane behavior of masonry enhanced with these modern techniques concerned mostly quasi-static (both monotonic and loading-unloading) or cyclic procedures, so to reproduce the effects of the wall inertial load; the common test arrangements concern 3 point bending [39], 4 point bending [33] or transversal uniform loads [40]. Some dynamic, shaking table tests were also performed [25]. Besides the experimental investigations, numerical models, ranging from micro to macro modelling approaches [46–58], were developed so to simulate the behavior of reinforced masonry (RM) walls and investigate the influence of the different parameters.

A FRM strengthening technique based on the application, on both sides of the wall, of a mortar coating with GFRP meshes embedded is considered in the paper. Recent experimental and numerical investigations evidenced its effectiveness in the seismic enhancement of unreinforced masonry (URM) buildings for in-plane actions [59–61]. The study herein presented focuses to out-of-plane actions and is aimed to the evaluation of the performances of masonry reinforced with this technique and to provide methods for the analytical design and numerical modelling purposes.

At first, the results of some experimental full scale out-of-plane four-point bending tests are presented and discussed, so to evidence the improvement of the masonry performances in terms of

resistance and deflection, due to the application of this strengthening technique. Moreover, the experimental results of some compression tests on masonry and of tensile tests on GFRP mesh reinforced mortar layers are illustrated, so to characterize completely the materials employed in the experimental campaign (in particular, the masonry Young modulus and the tension stiffening effect in the reinforcement). According to the approaches available in the literature [62–64], an analytical model similar to that used for reinforced concrete beams, based on deformation compatibility and force equilibrium, was applied to predict the cracking and ultimate bending moments of the strengthened specimens. A numerical model is then presented, so to predict the behavior of RM specimens. The numerical simulations are based on a bi-dimensional Finite Element, macro-model, so to simplify and accelerate the analysis; however the calibrated materials characteristics resulted applicable also in the case of a tri-dimensional model. The reliability of the models was proved by comparing the numerical results with the experimental ones.

2. Materials and methods

2.1. Reinforcement technique

The GFRP reinforced mortar coating technique (Fig. 1) consists in the application, on both faces of the masonry, of a thin layer of scratch coat, the execution of some passing through holes (25 mm diameter), the application of the GFRP mesh, the insertion, from both sides, of L-shaped GFRP connectors into the holes (200 mm lap splice) and injected with thixotropic epoxy resin and, finally, the application of a mortar coating (for a minimum thickness 30 mm). The GFRP mesh is formed with long fibers of Alkali-Resistant glass that are coated with a thermo-hardening resin (vinyl ester epoxy and benzoyl peroxide as catalyst); the composite wires are weaved to form the mesh by twisting the resin impregnated transversal fibers across the longitudinal wires. As to provide an adequate resistance against pull-out, the connectors are lap spliced inside the wall hole for a minimum of 200 mm. To improve the anchorage of the connector in the mortar layer, an additional GFRP mesh device is used.

The GFRP meshes available on the Italian market for the considered strengthening technique, have grid dimensions of 33×33 mm^2, 66×66 mm^2 and 99×99 mm^2 and have a net fiber cross section in a wire of 3.8 mm^2 (type "S") or 7.6 mm^2 (type "D"),

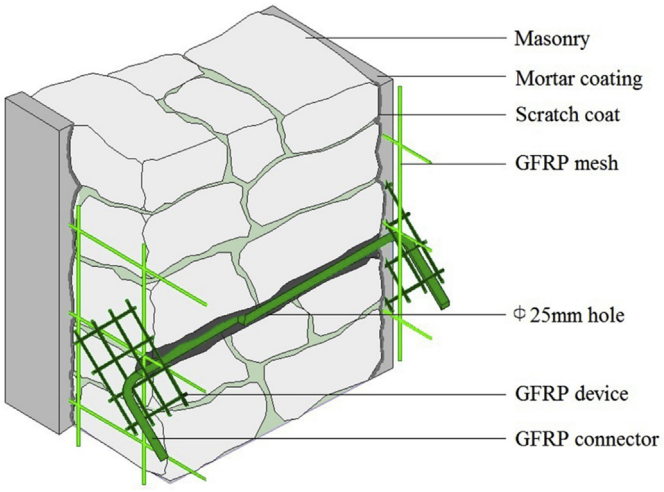

Fig. 1. Detailing of the GFRP reinforced mortar coating system.

for the last two meshes. The most commonly used GFRP mesh for in-plane strengthening of masonry walls is that with 66×66 mm^2 pitch and type "S" wire, so also in this study the same mesh was used.

The cross section of the GFRP connectors was 8×12 mm^2. The GFRP devices adopted to improve the anchorage of the connectors to the mortar coating were composed of square pieces of a GFRP mesh (grid pitch 33×33 mm^2); the global dimension of the device was 130×130 mm^2. The mechanical characteristics of the GFRP elements were assessed according to CNR DT 203:2006 [65], Appendix B, and are summarized in Table 1 in terms of equivalent cross section area ($A_{w,tot}$), fiber area ($A_{w,fib}$), tensile resistance (T_m), axial stiffness (EA) and coefficients of variation (c.o.v.).

Actually, different types of mortar may be utilized for the coating, such as natural binders, cement, pozzolanic additives [60], [66]. A lime and cement mortar commonly used for plaster (300 kg of hydraulic lime and 100 kg of cement per m^3 of mortar) was here considered for the reinforcement of masonry specimens subjected to out-of-plane bending tests. Compressive and flexural experimental tests on prismatic samples (40×40 mm^2 cross section, 160 mm length), performed in accordance to EN 196-1:2005 [67], evidenced for such a mortar an average compressive strength $f_{c,c} = 6.29$ MPa and a tensile strength $f_{t,c} = 1.10$ MPa. Moreover, compressive tests were performed on cylindrical mortar samples (100 mm diameter, 200 mm height) to evaluate the mortar Young modulus, according to "method B" proposed in EN 12390-13:2013 [68]: it resulted $E_c = 14430$ MPa.

According to the typical tests methods adopted for FRM systems [69], the global tensile behaviour of the reinforcement was investigated through experimental tensile tests on $900 \times 132 \times 30$ mm^3 mortar layers with 66×66 mm^2 grid GFRP mesh embedded (Fig. 2a). The test setup and results were described in detail and discussed in Ref. [70]. According to the mesh orientation in RM specimens subjected to bending, the GFRP twisted wires were disposed in the longitudinal direction of the samples. CFRP (Carbon fiber-reinforced polymers) strips, 180 mm length, glued with epoxy resin at both ends, were used as tabs. Two potentiometer transducers monitored the elongation during the loading procedure (base length 400 mm). Samples were tested at displacement control (rate 0.04 mm/mm in the un-cracked phase, 1.0 mm/mm in the cracked one).

The tensile load P vs. elongation Δl curves are reported in Fig. 2 b. A first, elastic branch was detected by the transducers, with stiffness dependent on the Young modulus of the mortar. Then, when the mortar tensile strength was exceeded, a first transversal crack formed, resulting in a sudden decrease of the load, which then increased again. When the tensile strength of the mortar is reached once more, a new crack is formed: about four cracks gradually appeared in the mortar, located, for the most, in correspondence of transversal mesh wires. Then, the material behaves approximately linearly, with a slope almost parallel to that of the GFRP wire alone, as evidenced in Fig. 2 b, where the load - displacement curve of two longitudinal GFRP wires having a 400 mm base length is reported. It is evidenced that the uncracked mortar among the cracks induced a stiffening of the behaviour of the layer in respect to that of the reinforcement only.

The specimens collapsed at the occurrence of the tensile rupture of the two longitudinal wires in correspondence of an average load of 11.32 kN (standard deviation 12% from the average value). It is evidenced that the average ultimate load resulted about 26% higher than that obtained from the characterization tests (Table 1). This was likely due to the different boundary condition applied on the GFRP wires; in fact in this case the presence of the transversal wires partially prevented the untwisting of the longitudinal wires, improving their tensile resistance.

Table 1
Characteristics of GFRP components: equivalent cross section area ($A_{w,tot}$), fiber area ($A_{w,fib}$), tensile resistance (T_m), axial stiffness (EA) and coefficients of variation (*c.o.v.*).

GFRP element	$A_{w,tot}$ [mm^2]	$A_{w,fib}$ [mm^2]	T_m [kN]	*c.o.v.* (T_m) [%]	EA [kN]	*c.o.v.* (EA) [%]
Parallel fibre wires	9.41	3.80	5.62	4.8	296	5.8
Twisted fibre wires	7.29	3.80	4.49	6.5	264	9.4
L-shaped connectors	96.0	57.6	36.01	2.9	–	–

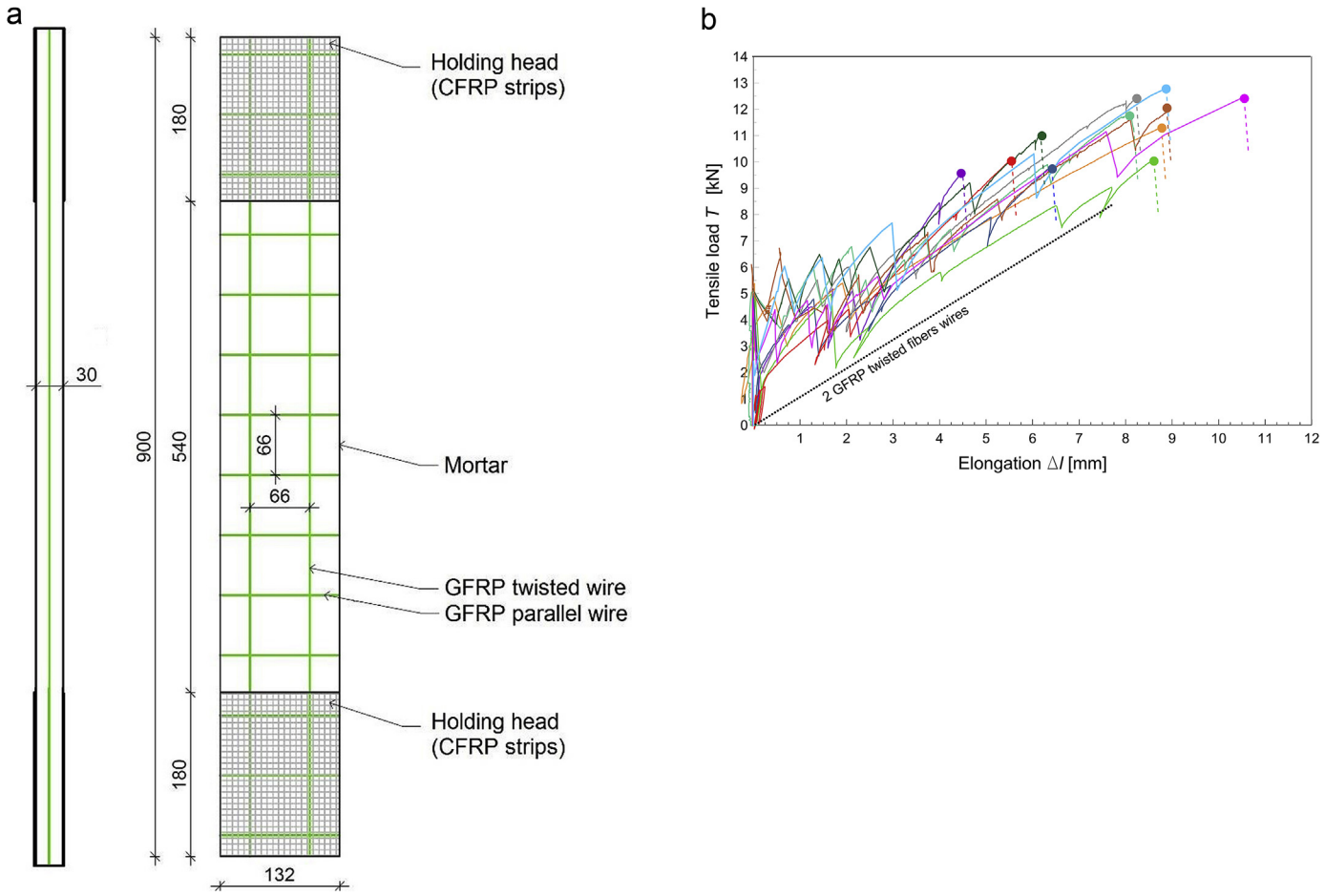

Fig. 2. Tensile tests on reinforced mortar layers: (a) characteristics of the specimens, (b) tensile load P vs. elongation Δl curves of the tested samples [70].

Bond tests were also performed, so to investigate on the masonry-mortar interaction [70]: three different bond length were considered: 120, 180 and 240 mm. In general, in the former case, the debonding of the mesh from the mortar matrix emerged. In the latter case, the failure for longitudinal wires rupture was obtained. In the intermediate case, different failure mechanism manifested (wires rupture, debonding of the mortar, debonding of the composite); however, similar loads, close to the wires resistance, were attained. Thus, it can be concluded that a bond length of at least 180 mm has to be guaranteed in order to exploit the maximum resistance of the considered reinforcement.

2.2. Specimens characteristics

The experimental campaign concerned wall specimens 3000 mm high and 1000 mm wide, of three different masonry types: solid brick (250 mm thick), rubble stones and cobblestones (400 mm thick, both). The three types of masonry considered are much diffused in the masonry buildings of a large part of Italy and of many European countries. One URM specimen and a RM one, strengthen with a GFRP reinforced mortar coating, were tested for each masonry type. 4 GFRP connectors per square meter were applied in RM specimen (Fig. 3).

The characteristics of the reinforcement were those described in section 2. In general, the minimum thickness of mortar coating applied in reinforced samples was 30 mm and the GFRP mesh was positioned at a distance of 15 mm from the external surface of the coating. It is observed that in solid brick masonry, the thickness of the mortar coating resulted approximately constant, due to the high planarity of the masonry surface; thus an average thickness about 30 mm can be assumed. Differently, in stone masonry, as the faces resulted more irregular, due to the blocks geometry an average thickness higher than 30 mm is expected. Actually, the roughness of the cobblestone masonry surface resulted higher than that of the rubble stone one: the average thickness of the mortar coating in rubble stone and cobblestones RM samples was estimated equal to 35 and 45 mm, respectively.

In solid brick masonry, the units (55 × 120 × 250 mm^3) were

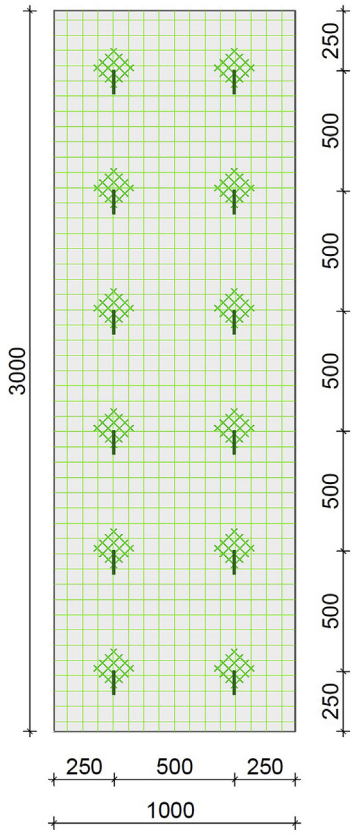

Fig. 3. Main geometrical characteristics of the tested specimens with positioning of the connections in reinforced samples.

arranged according to the header bond pattern (single leaf walls). The overlap, which was half the width of the brick, was obtained by introducing a three-quarter bat in each alternate course, at wall ends. The mortar joints had a 10 mm thickness. The bricks performed a compression resistance of 44.0 MPa (10 tests performed, c.o.v. 16%) [71]. In both the stone masonry types, the units were sandstones (density 2300 kg/m^3) and were arranged as close as possible so to limit the mortar joint dimensions. For rubble stones masonry, the unit dimensions were roughly 130 × 230 × 200 mm^3 (respectively height, width and depth); cobblestones specimens had elements with average dimensions 130 × 90 × 90 mm^3. Hydraulic lime mortars were employed: “type 1” for solid brick and rubble stone specimens (390 kg of binder per m^3 of mortar) and “type 0” for cobblestone ones (320 kg of binder per m^3 of mortar). Compressive and flexural characterisation tests on prismatic samples [67] provided, for the mortar type 1, an average compressive strength $f_{c,b}$ = 5.1 MPa and an average tensile strength $f_{c,b}$ = 1.1 MPa; for mortar type 0, it resulted $f_{c,b}$ = 3.1 MPa and $f_{c,b}$ = 0.7 MPa.

Compression tests were carried out on masonry samples 500 mm wide and 1000 mm high (Fig. 4): two concerned solid brick masonry (250 mm thick), two rubble stone (400 mm thick) and one cobblestones (400 mm thick) masonry.

The results are reported in Fig. 4 b in terms of compressive stress σ_c against average compressive strain ε_c curves. The Young modulus E_m was estimated as secant stiffness at 10% and 40% of the compressive strength $f_{c,m}$ (peak stress in the diagram). It emerged, on average, $f_{c,m}$ = 7.88 MPa E_m = 4266 MPa for solid brick masonry, $f_{c,m}$ = 4.51 MPa E_m = 2430 MPa for rubble stone masonry and $f_{c,m}$ = 1.04 MPa E_m = 1256 MPa for cobblestones masonry.

The samples were designed by using preliminarily the analytical relationships presented in section 4.1 (Eq. (3)), so that the RM flexural resistance ranged between 4 and 5 times that of the URM walls and verifying that other types of failures (due to shear in masonry or to FRM delamination from masonry) did not anticipate the RM collapse.

To distinguish the tested samples, an identifier composed of three parts is adopted: the first refers to the type of test (B for bending) and to the masonry group (B = solid bricks, R = rubble stones and C = cobblestones), the second identifies the type of masonry mortar (0 or 1) and the latter distinguishes unreinforced masonry (U) and masonry strengthened with the GFRP reinforced mortar coating technique (R).

2.3. Set-up and procedure

The bending tests (four point bending) were performed by applying two forces at the thirds of the height, with direction perpendicular to the wall surface. The steel reaction frame is illustrated in Fig. 5a-b: two horizontal beams, connected by vertical struts, were placed in contact with the top and the bottom ends of one wall face. On the opposite side, the horizontal loads were applied by two hydraulic jacks (142 kN each) contrasted by the steel frame and governed by an hand pump (maximum pressure 700 bar). The horizontal loading areas and the specimen base support were designed so to allow the wall rotation. The applied force was measured with a pressure transducer. To evaluate the actual deflection performances, potentiometer transducers were applied at the top and the bottom restraints and at the mid-height of the wall, on the wall face stressed in tension. Some additional transducers were placed on the compression stressed face, to check transversal expansions of the wall. All the potentiometers were fixed on a steel tripod, independent to the experimental apparatus. The force and the displacements were real-time monitored by connecting the measure equipment to an electronic acquisition unit interfaced with a computer. Loading-unloading cycles (steps 3−5 kN for plain specimens, 10 kN for the reinforced ones) were performed up to the occurrence of the first cracking; then the tests were prosecuted controlling the displacement.

3. Experimental results

The *P-δ* curves of the URM specimens, representing the total horizontal load against the out-of-plane net deflection at half height of the wall, are illustrated in Fig. 8 a. In the first part of the tests, the URM specimens did not exhibit any damage. Then, suddenly, the formation and rapid opening of a single crack occurred. The crack started from the tensed face of the samples (the front side), at about the mid-height of the wall and followed an approximately horizontal trend involving, mostly, a single bed joint. The crack affected, for the most, the masonry-mortar interface and involved the whole masonry thickness (Fig. 6). The P-*δ* curves exhibited an initial linear elastic trend, as the specimens remained undamaged. The peak load was reached, then, at the occurrence of the masonry crack, an abrupt decrease of the resistance emerged. The load rapidly dropped down to a residual value, which was maintained approximately constant till a deflection of 30 mm for BB-1-U and 50 mm for BR-1-U and BC-0-U. Then the tests were stopped, so to prevent the walls overturning. The initial slope of the P-*δ* curves, in the linear elastic phase, resulted quite similar for stone masonry samples and lower for solid brick specimen.

The *P-δ* curves of RM samples are plotted in Fig. 8b-d (also URM specimens curves are illustrated, for comparison): the envelope curves are reported, for graphic readability. RM samples (Fig. 7)

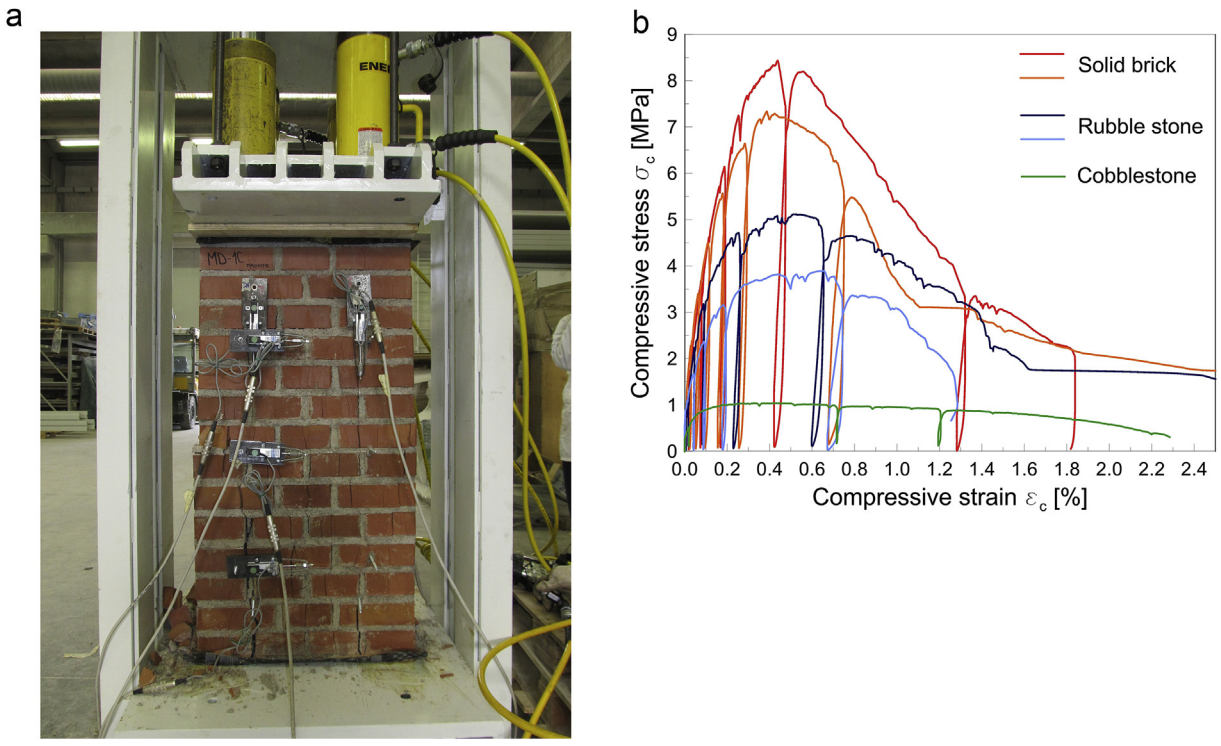

Fig. 4. Compression tests on masonry specimens: (a) test apparatus and (b) compressive stress σ_c vs. strain ε_c curves.

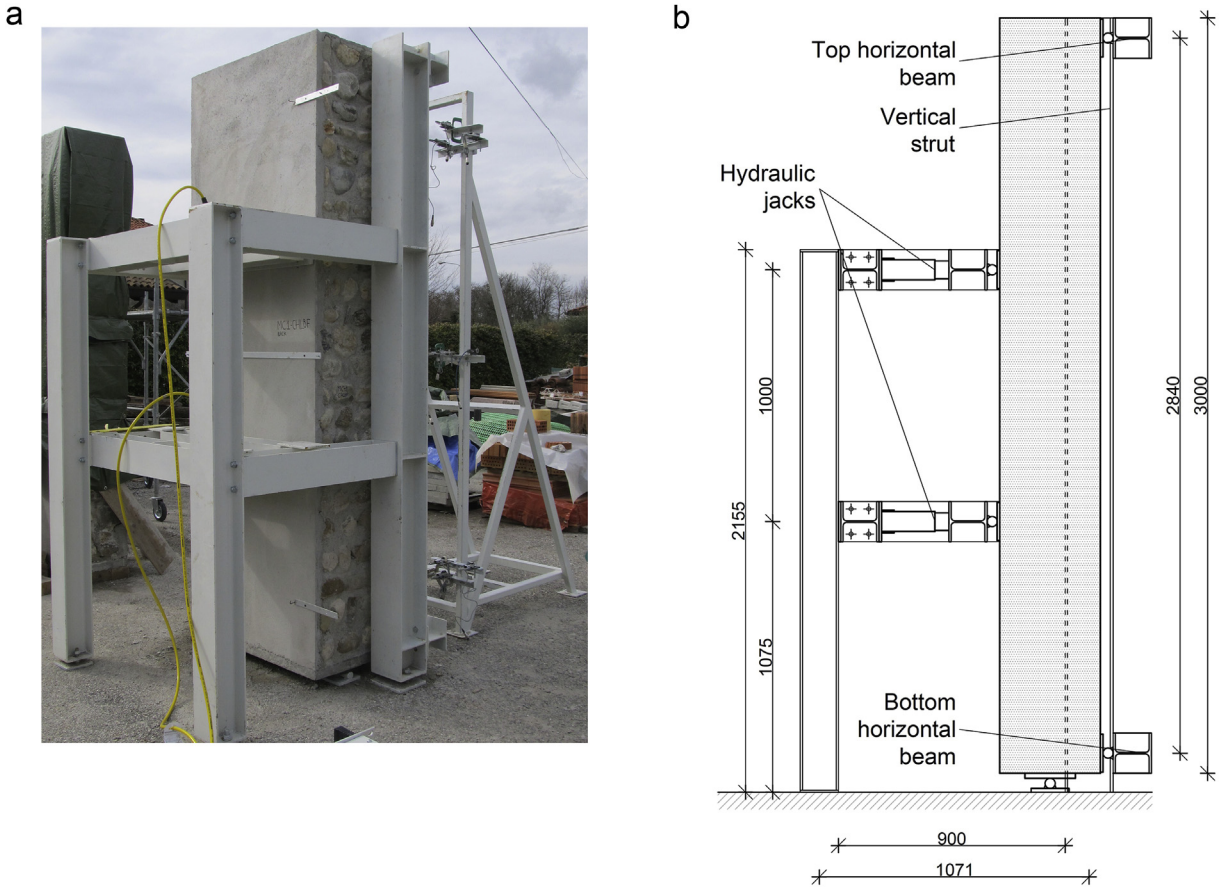

Fig. 5. Experimental apparatus for bending tests: (a) global view and (b) vertical section.

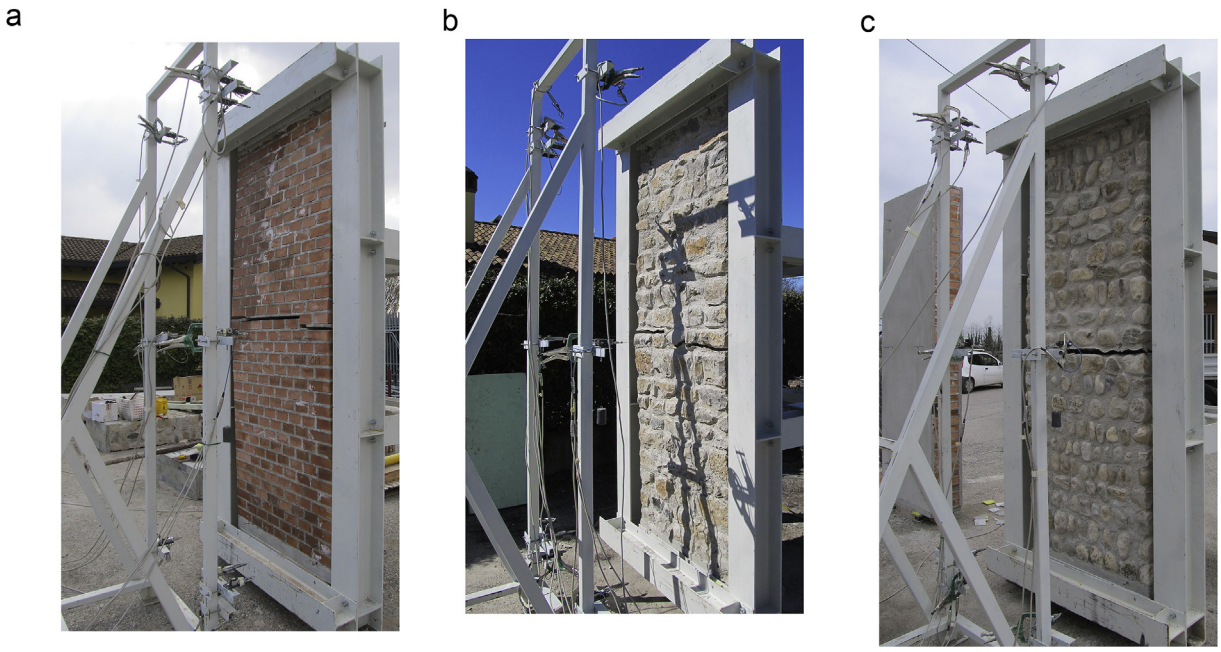

Fig. 6. URM samples at the end of the bending tests: (a) solid brick, (b) rubble stone and (c) cobblestones.

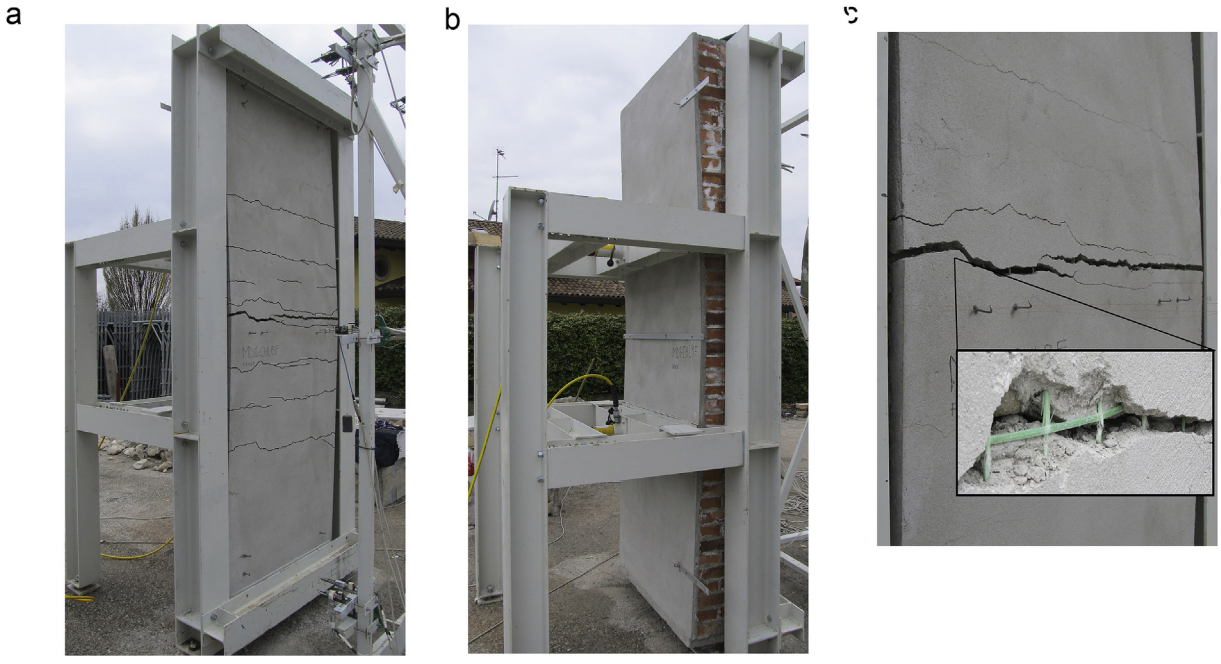

Fig. 7. Typical crack pattern of RM samples at the end of the bending tests: global views of (a) tensed and (b) compressed wall face and (c) detail of the GFRP wires rupture.

started to deflect remaining undamaged, until the opening of a first horizontal crack in the mortar coating, on the tensed wall face. Other horizontal cracks, almost parallel to the first one, gradually appeared. All cracks were concentrated approximately in the middle third of the wall height and progressively affected the whole coating thickness. The collapse occurred when, in correspondence of a crack, the vertical tensed wires of the GFRP mesh broke almost simultaneously (Fig. 7c). The tests were stopped in correspondence of a wall deflection of about 50 mm, so to prevent the walls overturning. The main crack (where the GFRP wires failure occurred) involved the whole masonry thickness (Fig. 7b) and, in solid brick RM sample, also part of the compressed mortar coating. However, the external mortar surface on the back side resulted undamaged at the end of all tests. In the P-δ curves of RM samples it can be distinguished a first, linear elastic branch (uncracked stage) and a cracking formation stage. To each crack formation was associated a drop of resistance, before to increase again. When the wires broke up, the load rapidly fall down to a residual value slightly greater than that obtained for URM samples.

Nor detachment of the coating neither damages on the compressed wall face were noted during the tests up to the GFRP wire rupture and the specimen collapse; the measured transversal

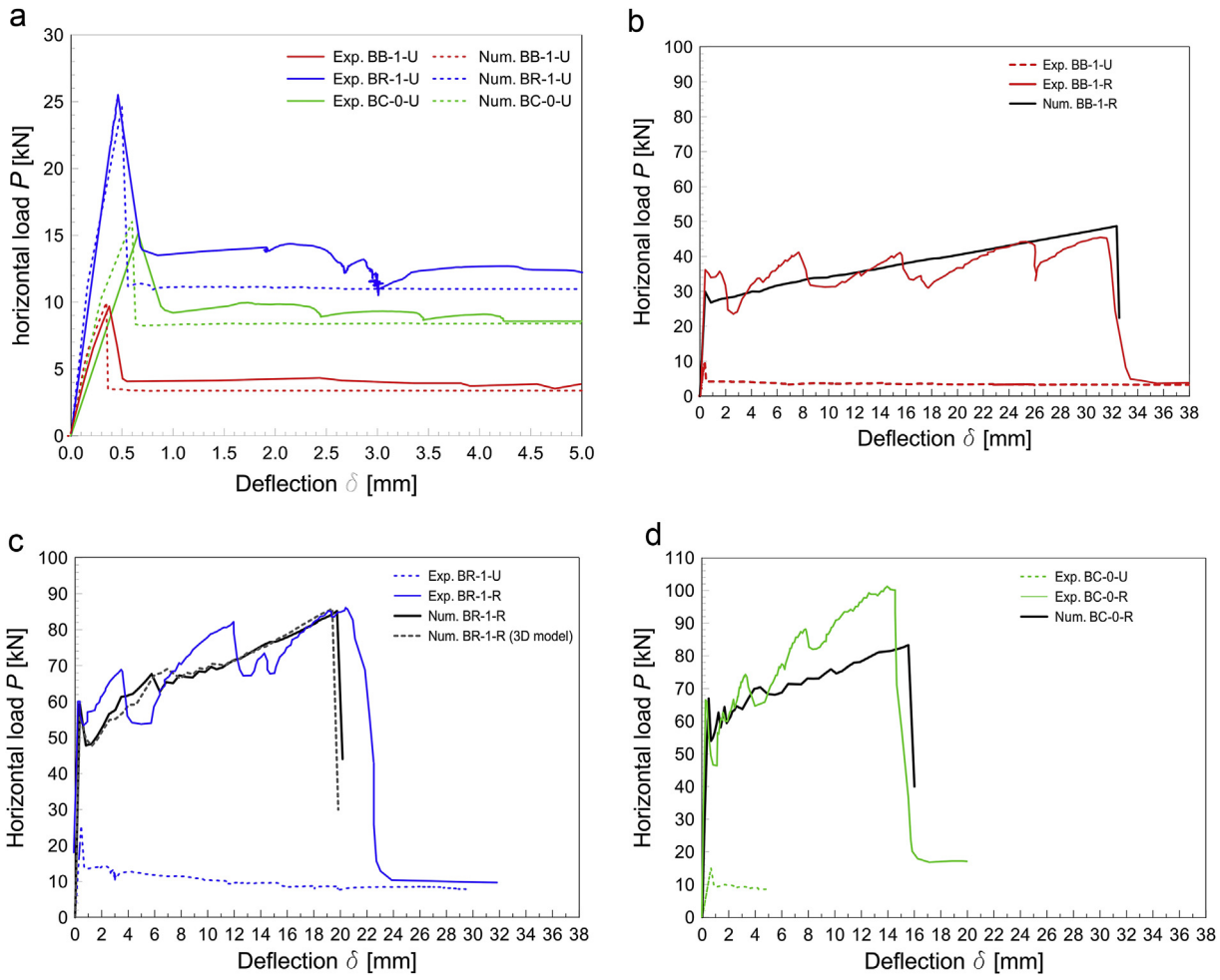

Fig. 8. Out of plane bending tests: horizontal load, P against deflection δ curves of (a) URM and RM specimens made of (b) solid brick, (c) rubble stone and (d) cobblestones.

expansion of the wall resulted always negligible.

The test main results in terms of first cracking load P_{cr}, maximum load P_u, out-of-plane deflection in correspondence of cracking δ_{cr} and maximum deflection δ_u are reported in Table 2. In the Table are also reported the values of the calculated bending moments associated to the first cracking M_{cr} and to the wall resistance M_u. In particular, these moments were derived from the value of the experimental load P (P_{cr} or P_u) assuming the simplified scheme reported in Fig. 9, which accounts also for a horizontal

Table 2
Main test results for out-of-plane bending tests in terms of load P, out-of-plane deflection δ and calculated bending moments M associated to first cracking (suffix "*cr*") and collapse (suffix "*u*") and ratios between the bending resistance of reinforced (R) and unreinforced (U) samples $M_{u(R)}/M_{u(U)}$.

Specimen ID	P_{cr} [kN]	P_u [kN]	δ_{cr} [mm]	δ_u [mm]	M_{cr} [kN*m]	M_u [kN*m]	$M_{u(R)}/M_{u(U)}$
Solid brick (250 mm thick)							
BB-1-U	9.55	9.55	0.38	0.38	3.69	3.69	–
BB-1-R	36.00	45.47	0.44	32.59	15.43	19.69	5.3
Rubble stone (400 mm thick)							
BR-1-U	25.52	25.52	0.46	0.46	10.35	10.35	–
BR-1-R	53.08	86.19	0.41	19.93	22.59	37.49	3.6
Cobblestone (400 mm thick)							
BC-0-U	15.14	15.14	0.56	0.56	5.79	5.79	–
BC-0-R	66.42	101.28	0.45	13.83	28.70	44.38	7.7

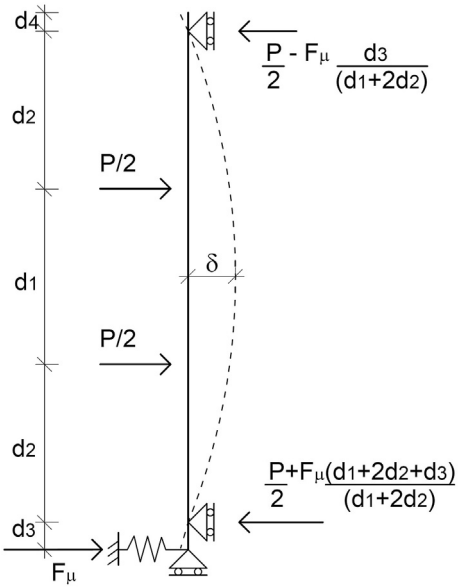

Fig. 9. Simplified scheme assumed for the four point bending test.

restraint due to friction (F_μ) at the base of the specimen (Fig. 5). For the evaluation of F_μ, the whole self-weight of the specimen was considered ($\gamma = 18$ kN/m^3 for solid brick masonry, $\gamma = 21$ kN/m^3 for rubble stone, $\gamma = 19$ kN/m^3 for cobblestone, and $\gamma = 20$ kN/m^3 for the reinforced mortar coating) and a friction coefficient of 0.74 was applied. Then the relationship used to derive bending moment is

$$M = \frac{P}{2} d_2 - F_\mu \frac{d_2 \cdot d_3}{(d_1 + 2d_2)}, \quad (1)$$

in which the parameters d_1 is the distance between loads, d_2 is the distance between the load and the support and d_3 is the vertical distance between the horizontal support and the vertical one at the base (Fig. 9).

The peak load of the solid brick URM specimen was 9.55 kN, while rubble stone and cobblestones specimens reached a value of 25.52 kN and 15.14 kN, respectively. The higher values obtained from stone masonry samples are reasonably related to the greater masonry thickness. Moreover, the lower resistance emerged in cobblestones sample, in respect to rubble stone one, is probably due to the weaker mortar and to the different stone blocks roughness and porosity, which may have influenced the block-mortar interface resistance. The residual resistance resulted of about 3.5 kN for solid brick sample, 9.0 kN for rubble stone one and 8.5 kN for cobblestones masonry.

The solid brick RM specimen cracked at 36 kN and reached a peak value of 45.5 kN in correspondence of a net deflection of 32.6 mm. The first cracking of the rubble stone sample occurred at 53.1 kN but then the load increased up to 86.2 kN, till a net deflection of 19.9 mm. In cobblestones specimen the first crack emerged at 66.42 kN and the maximum load was 101.28 kN (net deflection 13.8 mm). The higher resistance of cobblestone RM sample, in respect to rubble stone one resulted a little anomalous, considering the similar material characteristics of the two specimens. This difference may be attributable to some accidental greater frictional effect at the base.

The ratio between the bending resistance of RM and RM samples, $M_{u(R)}/M_{u(U)}$, was evaluated and reported in the last column of Table 2. It emerged that the masonry bending resistance of RM samples, with respect to that of URM specimens, increased to 5.3 times in solid brick walls, 3.6 times in those made with rubble stones and reaches 7.7 times in cobblestone specimen. The tests results also evidenced considerable increments in terms of deflection capacity, due to the presence of the GFRP mesh, which is essential for the wall resistance once the mortar coating cracks. In fact, the maximum deflection δ_u was not larger than $h/5000$ in URM walls, while in RM specimens ranged between $h/200$ and $h/100$.

No evident detachment between the masonry and the mortar, neither in tension coating (ends of the wall or close to bending cracks) nor in compression coating at mid-height (maximum bending moment). were noted during the tests up to the specimen collapse.

4. Analysis and discussion

4.1. Analytical predictions

As evidenced the experimental results of four point bending tests (Section 3), the stress state in the generic cross section of a specimen can be evaluated assuming the combined effect of the axial force, due to the masonry self-weight, and of the bending action induced by the two horizontal loads.

In RM walls, the superposition principle can be applied to estimate the value of the cracking moment, supposing no slip at materials interfaces, so the Bernoulli's principle applies (Fig. 10a):

$$M_{cr(R)} = \left(\frac{N}{A_{id}} + \frac{|f_{f,c}|}{\alpha_c} \right) \cdot W_{id} \quad (2)$$

A_{id} and W_{id} are the cross section area and the resistance modulus of the uncracked section idealized to masonry, $f_{f,c}$ is the flexural tensile strength of mortar coating and α_c is the modular ratio E_c/E_m. The presence of the GFRP wires can be assumed negligible with quite accuracy up to the crack formation in the mortar coating, due to the low geometrical percentage and to the low modular ratio.

The maximum bending moment (Fig. 10b) can be calculated considering a cracked section composed by only compressed mortar and by the tensed GFRP wires:

$$M_{u(R)}(N) = 0.8x \cdot f_{c,c} \cdot b \left(\frac{h_{TOT}}{2} - 0.4x \right) + n_w T_w \left(\frac{h_{TOT}}{2} - c \right)$$
$$\text{with} \quad x = \frac{N + n_w T_w}{0.8 f_{c,c} \cdot b} \quad (3)$$

n_w is the number of GFRP tensed wires in a cross section, T_w the tensile resistance of one wire, x the neutral axis depth, $f_{c,c}$ the compressive strength of the mortar of the coating, h_{TOT} and b the global depth and the width of the RM cross section and c the wires cover.

A comparison between experimental results and analytical predictions is reported in Table 3. The specific weights assumed for the masonry and for the mortar of the coating are those indicated in Section 3. According to the specimens characteristics (Section 2.2), a 30 mm thickness was assumed for the mortar in solid brick RM, 35 mm in rubble stone and 45 mm in cobblestones RM specimens. The flexural tensile strength of mortar coating $f_{f,c}$ is derived from its tensile strength $f_{t,c}$ through Equation (4) [72], in function of the global depth of the cross section h_{TOT} (in mm).

$$f_{f,c} = \max \left\{ (1.6 - h_{TOT}/1000) f_{t,c} \; ; \; f_{t,c} \right\} \quad (4)$$

The amount of GFRP tensed wires n_w was equal to 15 and the wire tensile resistance was derived from the tensile tests on GFRP reinforced layers (section 2). In particular, two different resistance

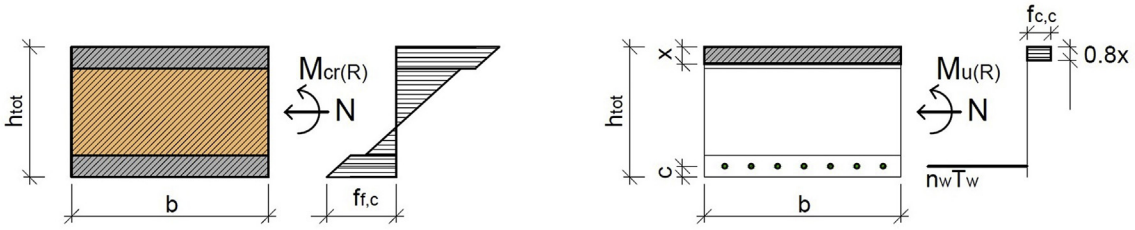

Fig. 10. Cross section for the calculation of (a) first cracking and (b) maximum bending moment in RM panels.

Table 3
Comparison between experimental (suffix "*exp.*") and analytical (suffix "*calc.*") results in reinforced panels in terms of first cracking M_{cr} and maximum bending moments M_u.

Specimen ID	Onset of cracking		GFRP mesh collapse		
	$M_{cr,exp}$ [kN*m]	$M_{cr,calc}$ [kN*m]	$M_{u,exp}$ [kN*m	$M_{u,calc(red)}$ [kN*m]	$M_{u,calc(inc)}$ [kN*m]
BB-1-R	15.43	14.76	19.69	22.30	27.88
BR-1-R	22.59	23.58	37.49	35.65	44.41
BC-0-R	28.70	26.11	44.39	37.15	46.31

values were considered ($T_{w,red}$ = 4.99 kN and $T_{w,inc}$ = 6.32 kN), reducing (*red*) or increasing (*inc*) the average strength ($T_{w,med}$ = 5.66 kN) by the standard deviation (0.67).

Low error percentages generally occurred (less than 16%) in the calculations of first cracking and also of the ultimate bending moment when a GFRP wire resistance of 4.99 kN is assumed. Diversely, consistent overestimations emerged for BB-1-R and BR-1-R when a resistance of 6.32 kN is considered for the GFRP wires, a good prediction resulted instead for BC-0-R. However, it is evidenced that the experimental ultimate moment $M_{u,exp}$ resulted quite anomalous in these latter case, as appreciably higher values than that emerged from BR-1-R, even though the masonry thickness and GFRP amount were equal in the two specimens.

By comparing equations (1) and (3), it is reasonable to deduce that, for the considered reinforcement, a decrease of the wall thickness leads to an increase of the effectiveness of the strengthening technique (ratio $M_{u(R)}/M_{u(U)}$), as emerged by comparing the results of solid brick and rubble stones samples. Moreover, a higher tensile resistance of the mortar coating or a thicker layer improve the first cracking load (equation (2)). Differently, considering that the GFRP mesh intervenes in the post-cracking stage, it is likely to note that a higher tensile strength of the mesh longitudinal wires improves the ultimate bending resistance (equation (3)), while a stiffer reinforcement, as well as a more effective mesh-matrix interaction (higher tension stiffening effect) limit the post-cracking ultimate deflection.

It is important to note that the presented analytical equations are based on the assumption of bending cracking and failure of RM. However, in general, the reinforced masonry shear resistance and the FRM delamination need to be checked, so to prevent these premature failures, which could not permit to exploiting the whole GFRP mesh resistance in tension.

In particular, the shear resistance V_{Rd}, neglecting the reinforcement contribute, can be prudentially ensured by applying the Jourawski theory and checking the respect of the inequality:

$$V_{Rd} = \frac{f_{v,Rd} \cdot b \cdot I}{S} = \frac{\left(f_{v,0} + \mu\sigma\right) \cdot b \cdot I}{S} \geq V_{Ed}(M_u), \quad (5)$$

where I is the second moment of area of the global cross section, S the first moment of area for half cross section and $V_{Ed}(M_u)$ the maximum shear acting when the bending resistance is attained. The masonry shear strength, $f_{v,Rd}$, can be evaluated by applying the Mohr-Coulomb failure criterion, considering the contribution of the masonry shear strength without axial loads ($f_{v,0}$, cohesion) and that due to friction related to the compressive stress σ acting in the cross section (μ coefficient of internal friction of masonry, typically 0.4).

The delamination of the FRM layer from the masonry surface can be avoided ensuring an adequate bond length at both wall ends. A prudential verification consists in assessing that, when the maximum bending resistance M_u is reached, the minimum distance l from the wall ends of the cross section in which the cracking bending moment M_{cr} is attained results higher of the minimum bond length $l_{b,min}$:

$$l\left(M_{cr(R)}\right) \geq l_{b.\min}. \quad (6)$$

The minimum bond length for the specific reinforced coating used has to be experimentally determined with a procedure as that presented in Ref. [54].

The main results of shear and delamination verifications for the three RM tested samples are resumed in Table 4. It is observed that, for the considered loading pattern (Fig. 9), the verifications were conducted referring to the upper end of the walls, thus $V_{Ed}(M_u) = M_u/d_2$ and $l(M_{cr}) = (M_{cr}/M_u{}^*d_2) + d_4$. d_4 is the distance from the upper wall end and the horizontal support (Fig. 9); the calculated values of $M_{cr,calc}$ and $M_{u,calc(inc)}$ (Table 3) were adopted.

In particular, for the masonry shear strength, the values of cohesion $f_{v,0}$ were derived from shove tests and diagonal compression tests [73]. The minimum bond length $l_{b,min}$ was deduced from some experimental results presented in Refs. [70] and [54], which provided early recommendations on the anchorage length necessary. In particular, as reported also at the end of subsection 2.1, a minimum bond length $l_{b,min}$ of 180 mm has to be guaranteed in order to exploit the maximum resistance of the considered reinforcement (GFRP wires rupture), avoiding both the premature detachment of the reinforced mortar coating from the masonry and the GFRP slippage from the mortar.

It emerged that both masonry shear and FRM delamination verifications resulted largely fulfilled.

4.2. Numerical simulations

A bi-dimensional finite element model (FEM) was elaborated using the software Midas FEA so to simulate the out-of-plane behaviour of URM and RM specimens and to investigate on the resisting mechanisms which form in the masonry walls. The characteristics of the FEM model and of the materials considered in the simulations are reported afterwards.

Considering the geometry of the experimental samples and the load pattern of the four point bending tests, a 2D model was at first preferred to a 3D one, for a preliminary study aimed to calibrate the different material parameters, so to reduce the time of analysis. However, a tri-dimensional model was then elaborated; the comparison on the results of the 2D and the 3D model proved that the bi-dimensional simplification is able to provide accurate results. The 3D model will permit to investigate on the out-of-plane behavior of actual masonry walls with openings or having a more articulated geometry.

4.2.1. Modelling and material characteristics

The 2D-model of the specimen was constructed using 4-node

Table 4
Masonry shear and FRM delamination checks for the three RM samples: masonry shear strength, $f_{v,Rd}$, second moment of area of the global cross section, V_{Rd}, maximum shear acting when $M_{u,calc(inc)}$ is attained, $V_{Ed}(M_u)$, calculated values of first cracking and maximum bending resistance, $M_{cr,calc}$ and $M_{u,calc(inc)}$, minimum distance from the wall end of the cross section where $M_{cr,calc}$ is attained, $l(M_{cr})$, and minimum bond length, $l_{b,min}$.

Specimen ID	Masonry shear			FRM delamination			
	$f_{v,Rd}$ [MPa]	V_{Rd} [kN]	V_{Ed} (M_u) [kN]	$M_{cr,calc}$ [kN*m]	$M_{u,calc(inc)}$ [kN*m]	l (M_{cr}) [mm]	$l_{b,min}$ [mm]
BB-1-R	0.2	41.33	30.98	14.76	27.88	529	180
BR-1-R	0.2	62.67	49.35	23.58	44.41	531	180
BC-0-R	0.2	65.33	51.46	26.11	46.31	564	180

plane strain elements both for the masonry and for the mortar coating. The height of the mesh elements was about 60 mm; the width was assumed 1/20 of the global element thickness for the masonry and 1/3 for the coating. A 66 mm thickness was considered for the plane strain element, so to represents the influence area of a single vertical GFRP wire (mesh wires spacing). The concrete element at the base and of the steel plates of the reaction frame in contact with the specimen were also modelled; 4-node plane strain elements were adopted for both. To guarantee the actual distribution of the horizontal load, a pinned nodded frame connecting the two loading areas was modelled and the horizontal displacement at the middle height of the frame was controlled.

According to the test setup (Section 2.3), the vertical translation was contrasted in the middle of the basement width and the horizontal displacement was constrained at the top and bottom plates, to simulate the contrast steel frame (Fig. 5). Moreover, the effect of the steel-to-steel friction ($\mu_s = 0.74$) in the contact points of the specimen with the steel frame was accounted.

The perfect adhesion between the mortar coating and the masonry was assumed, as no evident slip was noted in the experimental tests (Section 3). The GFRP vertical wires and the connectors were modelled by means of truss elements; the horizontal wires was neglected in the model.

Non−linear static analyses were performed by applying at first the whole self-weights and incrementing then step-by-step the imposed horizontal displacement. The Newton-Rapshon iterative method was considered (energy convergence criteria with a tolerance of 0.0001).

A smeared crack model [74] was considered both for the masonry and for the mortar coating. For the steel plates and the concrete basement an elastic behaviour was considered, with Young modulus equal to 210000 MPa and 32000 MPa, respectively, and Poisson modulus $\nu = 0.3$ and $\nu = 0.2$.

The specific weights assumed are 18 kN/m^3 for solid brick masonry, 21 kN/m^3 for rubble stone and 19 kN/m^3 for cobblestones. The masonry Young moduli E_m and compressive behaviour were deduced from the experimental compression tests (Section 2.2) and the Poisson modulus was equal to 0.2.

The masonry tensile strengths due to bending, $f_{f,m}$, were derived from the results of the experimental bending tests on URM specimens through the relationship:

$$f_{f,m} = \frac{N}{A} - M_{cr(U)}\frac{t/2}{I}, \tag{7}$$

where N/A is the uniform compressive stress induced by the self-weight of the masonry portion over the cracked section, I is the second moment of area, t the wall thickness and $M_{cr(U)}$ the bending resistance of the URM specimen (Table 2). An almost equal flexural strength $f_{f,m}$ was obtained for solid brick and rubble stone masonry specimens whereas it was significantly lower for cobblestones masonry specimen. This was due to the weaker mortar used in these latter case. In general, a ratio of 0.3 between the flexural strength $f_{f,m}$ and the tensile strength of mortar $f_{t,b}$ was surveyed.

The fracture energy of masonry in tension was calibrated through a parametric study conducted on URM specimens aimed to fit as close as possible the experimental results. The comparison between the experimental and numerical behavior of the URM specimens was reported in a load against deflection graph. The main points of the tensile relationships adopted for the different masonry types are summarised in Table 5. It is evidenced that higher values of residual resistance resulted for stone masonry types; this is in accordance to the greater interlocking effect between blocks.

Table 5
Constitutive relationships adopted for the tensile behaviour of the masonry.

Solid brick		Rubble stone		Cobblestone	
ε_t [‰]	σ_t [MPa]	ε_t [‰]	σ_t [MPa]	ε_t [‰]	σ_t [MPa]
0.000	0.000	0.000	0.000	0.000	0.000
0.057	0.320	0.117	0.360	0.138	0.190
0.090	0.055	0.150	0.100	0.220	0.050
0.150	0.009	0.290	0.022	0.350	0.010
0.500	0.009	0.500	0.022	0.500	0.010

The models were then completed with the reinforcement layers. The weight assumed for the mortar of the reinforcement was 20 kN/m^3; also for the coating, the Total Strain Crack criteria was adopted. The Young modulus E_c was 14430 (Section 2) and the Poisson ratio was equal to 0.2. For the compressive behavior, a simplified elastic relationship was considered, as no compressive plasticization of the mortar emerged in the experimental tests.

The tensile behavior of the mortar was derived from the tensile tests on GFRP reinforced mortar layers (Section 2), so to take into account for the tension stiffening effect of the mortar between two consecutive cracks. In particular, the mortar softening law, for a 30 mm thick mortar layer, was derived by converting the force − displacement curves in Fig. 2 b in stress − strain curve (Fig. 11), dividing the abscissas for the base length and the ordinates for the sample cross section. The line representing the longitudinal GFRP wires ($EA = 264$ kN - Table 1) was then subtracted to the average stress − strain behavior of the reinforced mortar coating deduced from experimental tests. The global tensile failure of the reinforced mortar coating was attained when a stress of 776 MPa was reached ($T_{w,med}/A_{w,tot} = 5.66$ kN/7.29 mm^2).

As evidenced in Section 2.2, the average mortar coating thickness was estimated equal to 30 mm in the solid brick RM specimens, 35 mm in rubble stone and 45 mm in cobblestones RM specimens. In the latter cases, the constitutive relationships of the mortar coating was adapted, applying the tension stiffening hyperbolic model proposed in Eurocode 2 [72] for steel reinforced concrete sections

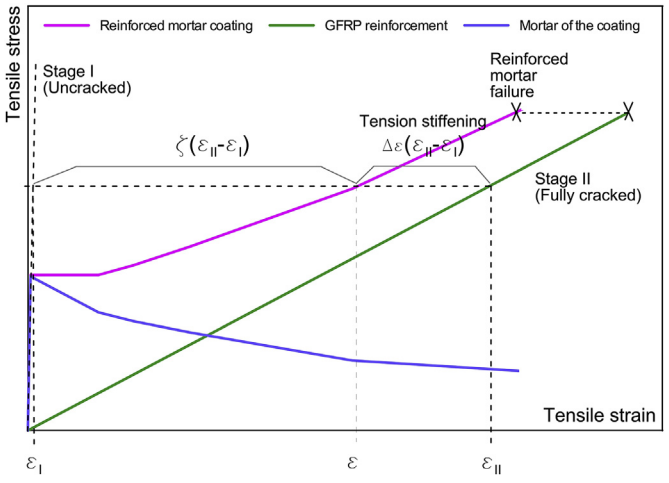

Fig. 11. Stress − strain behavior of the reinforced mortar coating, of the GFRP textile and of the mortar of the coating and indication of the main parameters considered in the tension stiffening model.

$$\varepsilon = \varepsilon_I + \xi \cdot (\varepsilon_{II} - \varepsilon_I) \quad with \quad \begin{cases} \xi = 0 & \text{for uncracked sections} \\ \xi = 1 - \beta \left(\frac{N_{cr}}{N}\right)^2 \leq 1 & \text{for cracked sections} \end{cases} \tag{8}$$

ε is the actual tensile strain, ε_I and ε_{II} are the values of strain calculated for the uncracked and fully cracked conditions, respectively, β is a constant accounting for the loading duration, N_{cr} represents the first cracking load and N the actual tensile force. According to such a model, the $\Delta\varepsilon$ represents the tension stiffening effect:

$$\Delta\varepsilon = \beta \left(\frac{N_{cr}}{N}\right)^2 (\varepsilon_{II} - \varepsilon_I). \tag{9}$$

It can be noted that, for thicker mortar coating, N_{cr} increases, thus a higher tension stiffening effect is expected. Comparing the tension stiffening effect of general mortar thickness with respect to that 30 mm thick through the relationship:

$$\frac{\Delta\varepsilon_{ti}}{\Delta\varepsilon_{t30}} = \left[\beta \left(\frac{f_{t,c} \cdot b \cdot t_i}{N}\right)^2 (\varepsilon_{II} - \varepsilon_I)\right] \Big/ \beta \left(\frac{f_{t,c} \cdot b \cdot t_{30}}{N}\right)^2 (\varepsilon_{II} - \varepsilon_I) \tag{10}$$

an increase of the tension stiffening effect of 1.36 and 2.25 times, respectively, for the 35 mm and the 45 mm thick mortar coating may be obtained. The main parameters considered in the tension stiffening model were indicated in Fig. 11. In general, it is observed that the mortar softening relationship, which accounts for the tension stiffening effect, is dependent from the adopted mesh dimension. The main points of the tensile stress σ_t against strain ε_t curves assumed for the mortar coating in the numerical models are reported in Table 6 for the different coating thicknesses.

For the 3D-model, identical mechanical characteristics were used for the different materials. 8-node solid elements were used for the masonry, for the mortar of the coating, for the concrete base element and for the steel plate of the reaction frame, instead of 4-node elements. The mesh elements were 60 mm height and 66 mm thick; the width was assumed 1/20 of the global element thickness for the masonry and 1/3 for the coating. Each single GFRP wire was modelled by means of truss element.

4.2.2. Comparison and analysis of results

The numerical results of URM and RM specimens were plotted in Fig. 8.

In the numerical models of URM samples (Fig. 8a) the first crack of the masonry always occurred at the height of the upper horizontal force, due to the combined effect of the compressive and bending action on a homogeneous material. Differently, the horizontal crack position in the experimental specimens varied between this zone and the mid-height of the wall, localizing in correspondence of the weaker interface section.

In Fig. 8 the numerical results of RM specimens were plotted in addition to the experimental curves referred to both RM and URM specimens. Both the first cracking and the GFRP wires rupture occurred at the height of the upper horizontal force. In solid brick (Fig. 8b) and in rubble stone (Fig. 8c) RM cases the cracking and the ultimate resistance points were estimated with good accuracy. Also the numerical behavior of the cobblestones RM specimen (Fig. 8d) evidenced a trend similar to the experimental one up to the occurrence of the first crack, but then the numerical curve prosecuted with a lower slope and a lower value of maximum load was reached. This aspect is probably due to the marked irregularity of the coating thickness, as the cobblestone masonry surface was significantly uneven, due to the round and irregular shape of the stone units. This aspect may alternate the tension stiffening effect of the mortar between cracks.

As an example, the 3D-numerical model was employed to simulate the behavior of specimen BR-1-R and the results are compared in Fig. 8 c. It is observed that the load − deflection capacity curve is in agreement with the results of the 2D-model, proving its reliability.

Table 6
Constitutive relationships adopted for the tensile behaviour of the mortar of the coating for the coating thicknesses considered.

30 mm thick		35 mm thick		45 mm thick	
ε_t [‰]	σ_t [MPa]	ε_t [‰]	σ_t [MPa]	ε_t [‰]	σ_t [MPa]
0.000	0.00	0.000	0.00	0.000	0.00
0.076	1.10	0.076	1.10	0.076	1.10
0.664	0.84	0.731	0.86	0.664	0.92
0.997	0.78	0.997	0.81	0.997	0.84
1.528	0.70	1.528	0.73	1.528	0.78
3.056	0.50	3.056	0.55	3.056	0.64
4.751	0.42	4.751	0.46	4.751	0.55
5.648	0.42	5.648	0.46	5.648	0.55

5. Conclusions

The paper deals with a technique for the seismic enhancement of historical masonry buildings consisting in the application of a GFRP mesh reinforced mortar coating on the wall faces. In particular, it focuses on its effectiveness against the out-of-plane masonry failure, investigating experimentally and numerically on the load carrying and displacement capacities on plain and reinforced masonry full-scale samples.

In particular, four point bending tests were performed considering three types of masonry (solid brick, rubble stone and cobblestone) and the failure mode of the specimens was analysed. Considering the onerousness of the samples, in full scale, one test on plain masonry and one on reinforced masonry were carried out for each masonry type. The aim was to obtain important information on the response of reinforced masonry subject to out-of-plane bending and understand the actual behavior of the reinforcement. It emerged that, in URM, the collapse occurred abruptly, due to the opening of a single horizontal crack, almost at mid-height of the specimen, at the interface between mortar joint and masonry units. In RM can be distinguished a first phase, until the first cracking in the mortar coating, in which the wall is almost intact, and a second phase, in which more horizontal cracks sequentially occur in the middle third of the height. The collapse occurs when, in correspondence of a crack, the GFRP wires reached their ultimate strain.

By comparing the resistances of RM and URM samples, emerged that strengthened specimens are able to resist to out-of-plane bending moments almost 5 times greater than that of plain specimens and can overcome to deflection ranging from 1/200 to 1/100 the wall height before collapse (while URM collapsed for very little deflections, up to 1/5000 the wall height). Actually the results are based on a limited number of specimens and a larger experimental programme would be necessary, but the experimental evidences are very clear that allow the authors to make the considerations reported.

An analytical study on RM walls showed that the cracking and the ultimate bending moment can be easily predicted using the well-known relationships used in the design of reinforced concrete beams subjected to combined axial and bending action for

uncracked and cracked sections, respectively.

A 2D numerical model was then developed so to comprehend the mechanical behaviour of RM walls. Four-node plane strain elements were utilized for the masonry and for the mortar of the coating, while the GFRP wires were modelled by means of truss elements. Nonlinear static analyses were performed by applying firstly the whole self-weights and incrementing then step-by-step the imposed out-of-plane displacement. Characterization tests were performed to assess the mechanical properties of the materials. In particular, the influence of the GFRP mesh on the reinforced mortar coating behavior was investigated experimentally through tensile tests, evidencing a not negligible tension stiffening effect on the GFRP wires of the mortar between adjacent cracks. The numerical simulation on URM specimens permitted to calibrate the dissipative capacity of the different masonry type (softening branch in tension).

The numerical results concerning RM samples resulted in agreement with the experimental ones, proving the reliability of the simulations. The possibility to extend the 2D model to a 3D model, based on the same material characteristics and on eight node solid elements instead of four-node plane strain elements, was also proved. The developed models will permit to perform parametric studies for the evaluation of the influence of the material characteristics on the RM walls global performances and to investigate on the behavior of some typical, actual configurations of masonry walls considering also the presence of overloads and wall constraints induced by storeys. Moreover, the 3D model will thus permit to investigate on the out-of-plane behavior of actual masonry walls with openings or having a more articulated geometry.

Acknowledgements

The research project was partly financed by the composite engineering factory FibreNet s.r.l., Pavia di Udine (UD), Italy. The useful help provided by Mr. Andrea Cernigoi, technician of the Testing Laboratory of the University of Trieste, during the execution of the tests is gratefully acknowledged.

References

[1] Gattesco N, Macorini L. In-plane stiffening techniques with nail plates or CFRP strips for timber floors in historical masonry buildings. Constr Build Mater 2014;58:64–76.
[2] Tomazevic M, Velechovsky T, Weis P. The effect of interventions in the floor structural system on the seismic resistance of historic-masonry buildings: an experimental study. In: Proceedings of the 10th WCEE. Madrid, July 19-24; 1992. pp.5312–5327.
[3] Chen SP. Out-of-Plane behavior of masonry walls strengthened with ferrocement. Adv Mater Res 2011;163–167:3545–50.
[4] Ashraf M, Khan AN, Ali Q, Shahzada K, Naseer A. Experimental behavior of full-scale URM building retrofitted with ferrocement overlay. Adv Mater Res 2011;255–260:319–23.
[5] Churilov S, Dumova-Jovanoska E. Analysis of masonry walls strengthened with RC jackets. In: Proceedings of the 15th world conference on earthquake engineering. Lisboa (P); 2012.
[6] Kadam SB, Singh Y. Mechanical properties of externally strengthened masonry. In: Proceedings of the 15th world conference on earthquake engineering. Lisbon (PT); 2012.
[7] Karantoni FV, Fardis MN. Effectiveness of seismic strengthening techniques for masonry buildings. J Struct Eng 1992;118(7):1884–902. ASCE.
[8] ElGawady M, Lestuzzi P, Badoux M. Seismic behavior of URM walls retrofitted using Shotcrete. In: Proceedings of the New Zealand society of earthquake engineering annual conference. At Napier (NZ); 2006.
[9] ElGawady M, Lestuzzi P, Badoux M. A review of conventional seismic retrofitting techniques for URM. In: Proceedings of 13th IB2MAC. Amsterdam, July 4-7; 2004.
[10] Valluzzi MR, Oliveira DV, Caratelli A, Castori G, Corradi M, De Felice G, et al. Round Robin Test for composite-to-brick shear bond. Mater Struct 2012;45:1761–91.
[11] Carrara P, Ferretti D, Freddi F. Debonding behavior of ancient masonry elements strengthened with CFRP sheets. Compos Part B Eng 2013;45:800–10.
[12] Velazquez-Dimas JI, Ehsani MR, Saadatmanesh H. Out-of-plane behaviour of brick masonry walls strengthened with fiber composites. ACI Struct J 2000;3:377–87.
[13] Albert ML, Elwi AE, Roger Cheng JJ. Strengthening of unreinforced masonry walls using FRPs. ASCE J Compos Constr 2001;5(2):76–84.
[14] D'Ambrisi A, Mezzi M, Caporale A. Experimental investigation on polymeric net-RCM reinforced masonry panels. Compos Struct 2013;105:207–15.
[15] Umair SM, Numada M, Amin MN, Meguro K. Fiber reinforced polymer and polypropylene composite retrofitting technique for masonry structures. Polymers 2015;7:963–84.
[16] Csikai B, Ramos LF, Basto P, Moreira S, Lourenço PB. Flexural out-of-panel retrofitting technique for masonry walls in historical constructions. In: Proceedings of the 9th international conference on structural analysis of historical constructions. Mexico city, 14–17 October; 2014.
[17] Borri A, Corradi M, Speranzini E, Giannantoni A. Consolidation and reinforcement of stone walls using a reinforced repointing grid. In: D'Ayala, Fodde, editors. Structural analysis of historic construction. London: Taylor & Francis Group; 2008. p.981–989.
[18] Schwegler G, Kelterborn P. Earthquake resistance of masonry structures strengthened with fiber composites. In: Proceedings of 11th WCEE. Acapulco, June 23-28; 1996. paper n.1460.
[19] Ehsani MR, Saadatmanesh H. Method of strengthening masonry and concrete walls with composite strap and high strength random fibers. U.S. Patent No. 5.640.825. Washington, D.C: United States Patents and Trademark Office; 1997.
[20] Triantafillou T. Strengthening of masonry structures using epoxy-bonded FRP laminates. J Compos Constr 1998;2(2):96–104.
[21] Papanicolaou C, Triantafillou T, Lekka M. Externally bonded grids as strengthening and seismic retrofitting materials of masonry panels. Constr Build Mater 2001;25(2):504–14.
[22] Gilstrap JM, Dolan CW. Out-of-plane bending of FRP-reinforced masonry walls. Comp Sci Technol 1998;58(8):1277–84.
[23] Willis CR, Yang Q, Seracino R, Griffith MC. Damaged masonry walls in two-way bending retrofitted with vertical FRP strips. Constr Build Mater 2009;23(4):1591–604.
[24] Anil O, Tatayoğlu M, Demirhan M. Out-of-plane behavior of unreinforced masonry brick walls strengthened with CFRP strips. Constr Build Mater 2012;35:614–24.
[25] Nezhad RS, Kabir MZ, Banazadeh M. Shaking table test of fibre reinforced masonry walls under out-of-plane loading. Constr Build Mater 2016;120:89–103.
[26] Hamed E, Rabinovitch O. Failure characteristics of FRP-strengthened masonry walls under out-of-plane loads. Eng Struct 2010;32(8):2134–45.
[27] Kashyap J, Willis CR, Griffith MC, Ingham JM, Masia MJ. Debonding resistance of FRP-to-clay brick masonry joints. Eng Struct 2012;41:186–98.
[28] Faella C, Camorani G, Martinelli E, Paciello SO, Perri F. Bond behaviour of FRP strips glued on masonry: experimental investigation and empirical formulation. Constr Build Mater 2012;31:353–63.
[29] Ghiassi B, Oliveira DV, Lourenço PB. Recent developments in durability of FRP-masonry systems. In: Proceedings of the international conference on rehabilitation and restoration of structures. Chennai, February 13-16; 2013. p. 107–16.
[30] Frigione M, Lettieri M, Mecchi AM. Environmental effects on epoxy adhesives employed for restoration of historical buildings. J Mater Civ Eng 2006;18(5):0899–1561.
[31] Karbhari VM, Chin JW, Hunston D, Benmokrane B, Juska T, Morgan R. Durability gap analysis for fiber-reinforced polymer composites in civil infrastructure. J Compos Construtions 2007;7:238–47.
[32] Ghiassi B, Marcari G, Oliveira DV, Lourenco PB. Water degrading effects on the bond behavior in FRP-strengthened masonry. Compos Part B Eng 2013;54:11–9.
[33] Galati N, Tumialan G, Nanni A. Strengthening with FRP bars of URM walls subject to out-of-plane loads. Constr Build Mater 2006;20(1–2):101–10.
[34] Korany Y, Drysdale R. Rehabilitation of masonry walls using unobtrusive FRP techniques for enhanced out-of-plane seismic resistance. J Compos Constr 2006;10(3):213–22.
[35] Turco V, Secondin S, Morbin A, Valluzzi MR, Modena C. Flexural and shear strengthening of un-reinforced masonry with FRP bars. Compos Sci Technol 2006;6(2):289–96.
[36] Galal K, Sasanian N. Out-of-Plane flexural performance of GFRP-reinforced masonry walls. J Compos Constr 2010;14(2):162–74.
[37] Dizhur D, Griffith M, Ingham J. Out-of-plane strengthening of unreinforced masonry walls using near surface mounted fibre reinforced polymer strips. Eng Struct 2014;59:330–43.
[38] Kashyap J, Willis CR, Griffith MC, Ingham JM, Masia MJ. Debonding resistance of FRP-to-clay brick masonry joints. Eng Struct 2012;41:186–98.
[39] Papanicolaou CG, Triantafillou TC, Papathanasiou M, Karlos K. Textile reinforced mortar (TRM) versus FRP as strengthening material of URM walls: out-of-plane cyclic loading. Mater Struct 2008;41(1):143–57.
[40] Ismail N, Ingham JM. In-plane and out-of-plane testing of unreinforced masonry walls strengthened using polymer textile reinforced mortar. Eng Struct 2016;118:167–77.
[41] Marcari G, Basili M, Vestroni F. Experimental investigation of tuff masonry panels reinforced with surface bonded basalt textile-reinforced mortar. Compos Part B Eng 2017;108:131–42.
[42] Gattesco N, Boem I, Dudine A. Behaviour of existing masonry strengthened

with a GFRP reinforced mortar coating. In: Proceedings of the 14th CC2013 conference. Cagliari, september 3-6; 2013. paper n.68.
[43] Bisby LA, Stratford T, Hart C, Farren S. Fire performance of well-anchored TRM, FRCM and FRP flexural strengthening systems. In: Proceedings of advanced composites in construction conference. Belfast (UK); 2013.
[44] Donnini J, De Caso y Basalo F, Corinaldesi V, Lancioni G, Nanni A. Fabric-reinforced cementitious matrix behavior at high-temperature: experimental and numerical results. Compos Part B Eng 2017;108:108–21.
[45] Alecci V, De Stefano M, Luciano R, Rovero L, Stipo G. Experimental investigation on bond behavior of cement-matrix–based composites for strengthening of masonry structures. J Compos Constr 2016;20(1):04015041.
[46] Manzoni E, Dusi A, Mezzi M. Polypmeric grid for a cost effective enhancement of the seismic performance of masonry buildings. In: Proceedings of the 14th world conference on earthquake engineering. Beijing (CN); 2008.
[47] Papanicolaou CG, Triantafillou TC, Papathanasiou M, Karlos K. Textile reinforced mortar (TRM) versus FRP as strengthening material of URM walls: out-of-plane cyclic loading. Mater And Struct 2008;41:153–7.
[48] D'Ambrisi A, Mezzi M, Caporale A. Experimental investigation on polymeric net-RCM reinforced masonry panels. Compos Struct 2013;105:207–15.
[49] Ismail N, Ingham JM. In-plane and out-of-plane testing of unreinforced masonry walls strengthened using polymer textile reinforced mortar. Eng Struct 2016;118:167–77.
[50] CNR DT 200 R1/2013. Guide for the design and construction of externally bonded FRP systems. Rome: CNR; 2013 [October].
[51] ACI 440.7R-10. Guide for design and construction of externally bonded FRP systems for strengthening unreinforced masonry structures. ACI Committee 440; 2010.
[52] Capozucca R. Effects of mortar layers in the delamination of GFRP bonded to historic masonry. Compos Part B Eng 2013;44:639–49.
[53] De Felice G, De Santis S, Garmendia L, Ghiassi B, Larrinaga P, Lourenco PB, et al. Mortar-based systems for externally bonded strengthening of masonry. Mater Struct 2014;4(2):16.
[54] Leone M, Aiello MA, Balsamo A, Carrozzi FG, Ceroni F, Corradi M, et al. Glass Fabric Reinforced Cementitious Matrix: tensile properties and bond performance on masonry sub-strate. Technical Report of the Rilem Committee 250-CSM “Composites for Sustainable Strengthening of Masonry”. 2016.
[55] Carbone I. Delaminazione di compositi a matrice cementizia su supporti murari. PhD Thesis. Rome (I): Università degli studi Roma TRE; 2010. in Italian.
[56] La Mendola L, Accardi M, Cucchiara C, Licata V. Nonlinear FE analysis of out-of-plane behaviour of masonry walls with and without CFRP reinforcement. Constr Build Mater 2014;54:190–6.
[57] Colombo M, Valente T, Barros JAO, Aprile A, Lourenço L. Fibre reinforced mortar application for out-of-plane strengthening of schist walls. Constr Build Mater 2016;121:185–97.
[58] Monaco A, Minafò G, Cucchiara C, D'Anna J, La Mendola L. Finite element analysis of the out-of-plane behavior of FRP strengthened masonry panels. Compos Part B Eng 2017;115:188–202.
[59] Gattesco N, Boem I, Dudine A. Diagonal compression tests on masonry walls strengthened with a GFRP mesh reinforced mortar coating. Bull Earthq Eng 2015;13(6):1703–26.
[60] Gattesco N, Boem I. Experimental and analytical study to evaluate the effectiveness of an in-plane reinforcement for masonry walls using GFRP meshes. Constr Build Mater 2015;88:94–104.
[61] Gattesco N, Boem I. Seismic enhancement of masonry buildings strengthened through GFRP reinforced mortar coating. Appl Mech Mater 2015;796:53–67.
[62] Mosallam AS. Out-of-plane flexural behavior of unreinforced red brick walls strengthened with FRP composites. Compos Part B Eng 2007;38:559–74.
[63] Derakhshan H, Griffith MC, Ingham JM. Out-of-plane behavior of one-way spanning unreinforced masonry walls. J Eng Mech 2012;139(4):409–17.
[64] Babaeidarabad S, Caso F, Nanni A. Out-of-Plane behavior of URM walls strengthened with fabric-reinforced cementitious matrix composite. J Compos Constr 2014;18(4):04013057.
[65] CNR DT 203/2006. Guide for the design and construction of concrete structures reinforced with fiber-reinforced polymer bars. Rome: CNR; 2007 [June].
[66] Gattesco N, Boem I. Influence of mortar coating type on the shear resistance of a GFRP based strengthening technique for brick masonry walls. In: Proceedings of the 16th IB2MAC. Padua, June 26-30; 2016. paper n.0267.
[67] EN 196–1. Methods of testing cement - Part 1: determination of strength. Brussels: CEN; 2005.
[68] EN 12390–13. Testing hardened concrete. Determination of secant modulus of elasticity in compression. Brussels: CEN; 2013.
[69] De Santis S, Carozzi FG, De Felice G, Poggi C. Test methods for textile reinforced mortar systems. Compos Part B Eng 2017 ISSN: 1359-8368. Available online.
[70] Gattesco N, Boem I. Characterization tests of GFRP reinforced mortar coating as a strengthening technique for masonry buildings. Compos Struct 2017;165:209–22.
[71] EN 772-1:2011+A1. Methods of test for masonry units - Part 1: determination of compressive strength. Brussels: CEN; 2015.
[72] EN 1992-1-1:2004/A1. Eurocode 2: design of concrete structures - Part 1-1: general rules and rules for buildings. Brussels: CEN; 2014.
[73] Gattesco N, Macorini L, Dudine A. Experimental response of brick-masonry spandrels under in-plane cyclic loading. J Struct Eng 2016;(2):142.
[74] TNO Building and Construction Research. DIANA – finite element analysis user's manual. 2002. Release 8.1 September.